Proceedings of the 2021 Winter Simulation Conference
S. Kim, B. Feng, K. Smith, S. Masoud, Z. Zheng, C. Szabo, and M. Loper, eds.

DEVELOPMENT OF A NEURAL NETWORK-BASED CONTROLLER FOR SHORT-RANGE ROCKETS

Raúl de Celis
Luis Cadarso

Aerospace Systems and Transport Research Group
European Institute for Aviation Training and Accreditation
Rey Juan Carlos University
Fuenlabrada
Madrid, 28943, SPAIN

ABSTRACT

Improving accuracy is a critical component of rocket-based defense systems. Accuracy may become independent of range when using inertial navigation systems. This is especially true for short-range man-portable air-defense systems, which are usually composed of portable missiles, whose movement is governed by non-linear and rapidly changing forces and moments. Effective guidance strategies for these systems could improve the weapon's precision. This research introduces a new non-linear neural network-based controller to improve navigation and control systems by lowering the circle error probable, which is a measure of accuracy. Nonlinear simulations based on actual flight dynamics are used to train the neural networks. The simulation results show that the presented approach performs well in a 6-DOF simulation environment, featuring high accuracy and robustness against parameter uncertainty.

1 INTRODUCTION

Navigation signals from Global Navigation Satellite Systems (GNSS) are widely used in defense systems nowadays. Regrettably, their reliability usually decreases inversely proportional to mission requirements. It should be noted that GNSS signal attenuation and loss results in a reduced signal/noise relationship. Although Inertial Navigation Systems (INS), such as Inertial Measurement Units (IMUs), are independent of external perturbations, they have significant flaws such as inertial sensor (gyro and accelerometer) imperfections that cause cumulative errors, incorrect navigation system initialization, and flaws in the gravity model implemented, especially for long ranged flights. But, in this last case, INS are an excellent source of navigation information when combined with GNSS receivers, which can reduce INS errors (de Celis et al. 2017).

Man-portable air-defense systems are shoulder-launched missiles. They are typically guided weapons that are used to reduce the threat posed by low-flying aircraft, particularly helicopters. Different techniques, such as infrared and laser, can be used to guide these weapons. These systems can also be used for surface-to-surface defense where target location knowledge is known and laser or infrared guiding could not be required. In such a case, INS combined with GNSS receivers can suffice as a source of information. However, typical man-portable air-defense systems feature short range and flight times, making successful reception of the GNSS signal impossible. Note that, if there are not additional sources of external information, due to limitations on costs, project scope, or mission requirements, precision must be achieved using only on-board systems and loaded information before launch.

Whatever the system's architecture, cost, precision, and robustness are critical characteristics. They are, however, diametrically opposed goals. Precision aims to reduce "collateral damage". High values for this

978-1-6654-3311-2/21/$31.00 ©2021 IEEE

damage can make military action unfeasible (Hamilton 1995). Robustness is the result of an all-weather and all-terrain system, i.e., a system that does not degrade regardless of the operating conditions. It is always difficult to obtain a system with high precision and robustness at a low cost.

The need for new Guidance, Navigation, and Control (GNC) systems has prompted research into the stability and controllability of aerial platforms (de Celis et al. 2017). Based on missile proportional navigation, Zhao and Zhou (2015), Creagh and Mee (2010) presents cooperative strategies for multiple missiles based on the traditional Proportional Navigation (PN). In Lee et al. (2001), an attitude control system for a spinning sounding rocket is designed, which includes a proportional, integral, and derivative (PID) type controller. Proportional-derivative navigation guidance laws for the terminal phase are proposed in Lechevin and Rabbath (2012), Wang et al. (2015). The line of sight is reconstructed in Nesline and Zarchan (1985). A finite-time convergent sliding-mode guidance law with terminal impact angle constraint is presented in Zhang et al. (2012). Theodoulis et al. (2013) presents a complete design for the guidance and autopilot modules for a class of spin-stabilized fin-controlled projectiles.

If GNSS signals are available, expensive inertial navigation systems can be replaced with less precise devices to save money while maintaining an acceptable level of precision. This would enable the inertial system to be updated at a low cost, reducing the growth of errors. In addition, merging the signals of several low-cost sensors, which improves overall accuracy, can be a good strategy for reducing costs and collateral damage. The advantages of integrated data fusion have been demonstrated in a variety of antisubmarine, strategic air, and land warfare applications (Waltz and Buede 1986). Data fusion algorithms for six degrees of freedom missiles are described in Nguyen et al. (2016). The benefits and drawbacks of using various types of INS enhanced with GNSS updates have been considered by Schmidt and Phillips (2011). In addition to INS/GNSS hybridization, a group of nonlinear observers are described by Bryne et al. (2017). If additional sensors are available, they may be additional contributions to a filter, for example, the Kalman filter (de Celis et al. 2017).

However, even in GNSS/IMU integrated systems, many scenarios feature high uncertainty, unknown disturbances, and abnormal measurements, which may be especially prominent during terminal guidance for low-cost devices. As a result, developing new robust algorithms that can achieve the required accuracy levels at a low cost during guidance is a critical component of projectile research, even more if GNSS signals are not available. Modern laser guided ballistic rockets, for example, integrate IMU, GPS, and laser guidance capability, providing high precision and all-weather attack capability (de Celis and Cadarso 2019; Zhang et al. 2017).

A current need is for new methodologies and algorithms that aim to propose effective and robust systems that allow for a high level of autonomy and precision at a low cost. A promising methodology in this regard is what is known as machine learning. It provides a plethora of possibilities and revolutionary solutions that are particularly appealing for GNC applications, where its foray is still new and shallow, but undeniably promising. Indeed, using machine learning methods for parameter estimation based on the dynamics of aerospace vehicles has the advantage that once the algorithm is trained or calibrated, it is not necessary to understand the physical-mathematical foundations that govern dynamics, but it is the algorithm that, for the input data, returns the information that can later be used within the GNC algorithm (Solano-López et al. 2019; Mohamed and Dongare 2018; Alameri 2019; Satir et al. 2021; Diwani et al. 2020).

The goal of this paper is to improve existing control methods by employing an efficient algorithm based on a neural network. This is achieved by intelligently determining controller parameters during the flight using only information from IMUs.

1.1 Contributions

This scientific research's main contribution is the proposal of neural networks to implement guidance, navigation and control systems for a short-range artillery rocket where GNSS signals are not a viable option. This is achieved by predicting the required deflection of the rocket actuators solely using data

provided by an IMU, thereby improving accuracy at the point of impact. The main advantage of this advancement over the traditional one is that accuracy can be auto-improved during the neural network learning process.

The proposed method is based on neural networks that predict the required movement of the canard actuators on the man-pad rocket. The magnitudes measured by the IMU are used as inputs for neural networks, and the required deflections of each of the four canard actuators are the outputs. This neural network-based approach is capable of handling the significant coupling between lateral and normal rocket nonlinear dynamics.

To build a realistic simulation campaign, it is proposed to use a flight dynamics model that reproduces a highly dynamic rocket and takes into account non-linearities in aerodynamic forces and moments. The simulation results demonstrate the accuracy and applicability of these algorithms in non-deterministic environments, launch conditions, and projectile conditions.

This paper is organized as follows: Section II describes the system modeling in detail. Algorithms for navigation, guidance, and control are covered in Section III. Section IV reveals the outcomes of simulations. Finally, there is a discussion and conclusion.

2 SYSTEM MODELING

This section focuses on the description of the plant, the non-linear flight mechanics model, actuation and sensor models used for navigation purposes.

2.1 Rocket Definition

The proposed guidance, navigation and control approach is applied to a 65 mm axis symmetric man-pad rocket (de Celis et al. 2017). The rocket features extending canard control fins, and stabilizing rear wings (see Figure 1). The maneuvering mechanism consists of a fuse attached to the tip of the rocket. It is made up of four canard surfaces, decoupled two by two, to generate a control force in an orthogonal plane to the rocket section, and its associated moment.

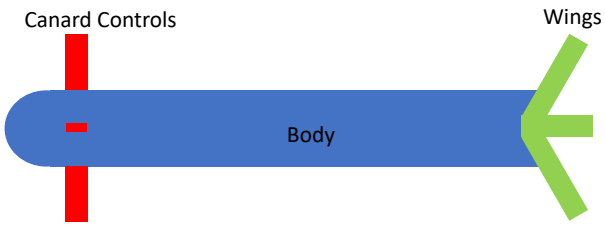

Figure 1: Rocket configuration.

Thrust profile is shown in Figure 2 and mass and aerodynamic data for the rocket are shown in Table 1 and Table 2, respectively. Note that I_{x0} and I_{y0} are initial inertia moments, X_{CG0} is the initial longitudinal position of the center of mass (measured from the tip), $C_{D_0}(M)$ is drag force linear coefficient, $C_{D_{\alpha^2}}(M)$ is drag force square coefficient, α is total angle of attack, $C_{L_\alpha}(M)$ is lift force linear coefficient, $C_{L_{\alpha^3}}(M)$ is lift force cubic coefficient, $C_{mf}(M)$ is Magnus force coefficient, $C_{Nq}(M)$ is pitch damping force coefficient, $C_{M_\alpha}(M)$ is overturning moment linear coefficient, $C_{M_{\alpha^3}}(M)$ is overturning moment cubic coefficient, $C_{M_q}(M)$ is pitch damping moment coefficient, $C_{mm}(M)$ is Magnus moment coefficient, $C_{spin}(M)$ is spin damping moment coefficient, and $C_{N\delta}(M)$ is the canard force coefficient. All the values for these parameters are based either on experimental measurements, or on fluid dynamics numerical simulations and wind tunnel verification. To keep continuity and derivability of thrust and aerodynamic profiles, with respect to time and Mach number, respectively, a cubic spline interpolation is employed.

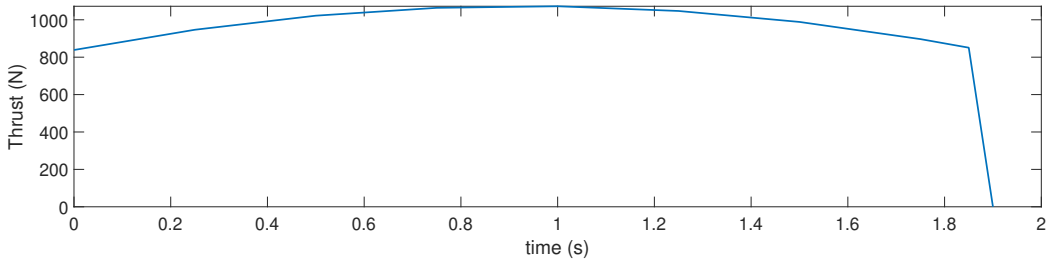

Figure 2: Thrust profile vs. time.

Table 1: Thrust and mass rocket parameters.

Parameter	Initial mass	Propellant mass	I_{x0}	I_{y0}	X_{CG0}	Caliber
Value	7.00 kg	1.50 kg	0.01 kgm^2	0.25 kgm^2	0.45 m	0.065 m

Table 2: Aerodynamic rocket parameters for different Mach numbers.

M	$C_{D_0}(M)$	$C_{D_{\alpha^2}}(M)$	$C_{L_\alpha}(M)$	$C_{L_{\alpha^3}}(M)$	$C_{mf}(M)$	$C_{Nq}(M)$	$C_{M_\alpha}(M)$	$C_{M_{\alpha^3}}(M)$	$C_{M_q}(M)$	$C_{mm}(M)$	$C_{spin}(M)$	$C_{N\delta}(M)$
0.00	0.51	6.87	8.82	-17.51	-0.54	22.88	-4.09	25.75	-30.22	0.88	-9.72	1.74
0.20	0.51	6.87	8.82	-17.51	-0.54	22.88	-4.09	25.75	-30.22	0.88	-9.72	1.74
0.60	0.58	7.04	9.71	-23.35	-0.64	25.92	-4.58	31.80	-35.08	1.05	-10.72	1.93
0.70	0.60	7.12	9.90	-24.27	-0.66	26.64	-4.13	28.95	-36.30	1.09	-10.80	2.03
0.80	0.63	7.21	10.07	-24.91	-0.68	27.42	-3.70	26.41	-37.72	1.13	-10.85	2.10
0.88	0.72	7.24	10.13	-24.98	-0.70	27.95	-3.45	25.08	-38.90	1.16	-10.85	2.10
0.90	0.79	7.23	10.13	-24.98	-0.71	28.13	-3.35	24.61	-39.33	1.17	-10.85	2.10
0.93	0.98	7.15	10.09	-24.93	-0.72	28.25	-3.26	24.13	-39.79	1.18	-10.85	2.10
0.95	1.11	7.11	10.07	-24.91	-0.72	28.41	-3.16	23.63	-40.26	1.19	-10.85	2.10
1.00	1.32	9.95	10.06	-6.45	-0.73	28.79	-2.96	26.42	-41.28	1.21	-10.85	2.10

2.2 Flight Dynamics Model

To construct the flight dynamics model, two axes systems are defined: body axes and earth axes. Sub index b defines the body axes. x_b points forward and it is embedded in the rocket's plane of symmetry, z_b is perpendicular to x_b and points down, also embedded in the rocket's plane of symmetry. y_b forms a clockwise trihedron. The origin of the body axes is at the rocket's center of mass. Earth axes, also known as North-East-Down axes (NED) are defined by sub index e. x_e pointing north, z_e perpendicular to x_e and pointing nadir, and y_e forming a clockwise trihedron. All forces and moments are to be expressed in these axes, with the aim of obtaining flight dynamics and actuation equations. The following expressions, 1 to 5 have been tested and verified against real ballistic trajectories as it is explained in de Celis et al. (2017), de Celis and Cadarso (2018).

Total external forces and moments for the rocket are given in 1:

$$\left[\overrightarrow{F_{ext}} \quad , \quad \overrightarrow{M_{ext}} \right] = \left[\overrightarrow{D} + \overrightarrow{L} + \overrightarrow{M} + \overrightarrow{P} + \overrightarrow{T} + \overrightarrow{W} + \overrightarrow{C} + \overrightarrow{CF} \quad , \quad \overrightarrow{O} + \overrightarrow{P_M} + \overrightarrow{M_M} + \overrightarrow{S} + \overrightarrow{CM} \right], \quad (1)$$

where $\overrightarrow{D}$ is drag force, $\overrightarrow{L}$ is lift force, $\overrightarrow{M}$ is Magnus force, $\overrightarrow{P}$ is pitch damping force, $\overrightarrow{T}$ is thrust force, $\overrightarrow{W}$ is weight force, $\overrightarrow{C}$ is Coriolis force, $\overrightarrow{CF}$ is actuators control force, $\overrightarrow{O}$ is overturn moment, $\overrightarrow{P_M}$ is pitch damping moment, $\overrightarrow{M_M}$ is Magnus moment, $\overrightarrow{S}$ is spin damping moment and $\overrightarrow{CM}$ is actuators control moment.

Rocket forces in body axes are described in 2 and 3. They include contributions from drag, lift, Magnus, pitch damping, thrust, weight, control and Coriolis forces:

$$\begin{bmatrix} \overrightarrow{D} & , & \overrightarrow{L} \\ \overrightarrow{M} & , & \overrightarrow{P} \\ \overrightarrow{CF} & & \end{bmatrix} = -\frac{\pi}{8} d^2 \rho \begin{bmatrix} \left(C_{D_0}(M) + C_{D_{\alpha^2}}(M)\alpha^2\right) \|\overrightarrow{v_b}\| \overrightarrow{v_b} & , & \left(C_{L_\alpha}(M)\cdot\alpha + C_{L_{\alpha^3}}(M)\alpha^2\right) \left(\|\overrightarrow{v_b}\|^2 \overrightarrow{x_b} - (\overrightarrow{x_b}\cdot\overrightarrow{v_b})\overrightarrow{v_b}\right) \\ d\frac{C_{mf}(M)}{I_x}\left(\overrightarrow{L_b}\cdot\overrightarrow{x_b}\right)(\overrightarrow{x_b}\times\overrightarrow{v_b}) & , & -d\frac{C_{Nq}(M)}{I_y}\|\overrightarrow{v_b}\|^2 \left(\overrightarrow{L_b}\times\overrightarrow{x_b}\right) \\ \sum_{i=1}^{i=4}\left(C_{N\delta}(M)\delta_i\cdot\overrightarrow{n_{b_{\delta_i}}}\right) & & \end{bmatrix} \tag{2}$$

$$\begin{bmatrix} \overrightarrow{T} & , & \overrightarrow{W} & , & \overrightarrow{C} \end{bmatrix} = \begin{bmatrix} T(t)\overrightarrow{x_b} & , & m\overrightarrow{g_b} & , & -2m\overrightarrow{\Omega}\times\overrightarrow{v_b} \end{bmatrix}, \tag{3}$$

where d is rocket caliber, ρ is air density, $\overrightarrow{L_b}$ is rocket angular momentum in body axes, I_x *and* I_y are rocket inertia moments in body axes, $\overrightarrow{x_b}$ is rocket nose pointing vector in body axes, δ_i is the deflection angle for each canard i, $\overrightarrow{n_{b_{\delta_i}}}$ is the normal vector to each canard i, $\overrightarrow{g_b}$ is gravity vector in body axes, $\overrightarrow{\Omega}$ is earth angular speed vector, and $\overrightarrow{v_b}$ is rocket velocity in body axes.

Rocket moments, which include overturning, pitch damping, Magnus, spin damping and control, are showed in 4:

$$\begin{bmatrix} \overrightarrow{O} & , & \overrightarrow{P_M} \\ \overrightarrow{M_M} & , & \overrightarrow{S} \\ \overrightarrow{CM} & & \end{bmatrix} = \frac{\pi}{8} d^3 \rho \begin{bmatrix} \left(C_{M_\alpha}(M) + C_{M_{\alpha^3}}(M)\alpha^2\right)\|\overrightarrow{v_b}\|^2 (\overrightarrow{v_b}\times\overrightarrow{x_b}) & , & \frac{1}{I_y}C_{M_q}(M)\|\overrightarrow{v_b}\| \left(\overrightarrow{L_b} - \left(\overrightarrow{L_b}\cdot\overrightarrow{x_b}\right)\overrightarrow{x_b}\right) \\ -\frac{d}{I_x}C_{mm}(M)\left(\left(\overrightarrow{L_b}\cdot\overrightarrow{x_b}\right)((\overrightarrow{v_b}\cdot\overrightarrow{x_b})\overrightarrow{x_b}) - -\overrightarrow{v_b}\right) & , & \frac{d}{I_x}C_{spin}(M)\|\overrightarrow{v_b}\|\left(\overrightarrow{L_b}\cdot\overrightarrow{x_b}\right)\overrightarrow{x_b} \\ \sum_{i=1}^{i=4}\left(C_{N\delta}(M)\frac{C_{L\alpha}(M)}{C_{M\alpha}(M)}\delta_i\cdot\left(\overrightarrow{i_b}\times\overrightarrow{n_{b_{\delta_i}}}\right)\right) & & \end{bmatrix}, \tag{4}$$

Once the mathematical models for forces and moments are given, the equations of motion dynamics for the rocket are formulated using a Newton-Euler approach. These equations are shown in 5. To relate the reference systems, namely flat-Earth coordinate system (denoted by frame e) and the body-fixed coordinate system b, Euler angles are employed: roll (ϕ), pitch (θ), and yaw (ψ) angles.

Note that all the presented mathematical expressions are nonlinear. For example, aerodynamic linear, quadratic, and cubic coefficients depend on Mach number, which varies along the rocket flying performance. Also notice that, it is assumed that fuse mass is negligible, which practically means the reactions between fuse and aft part of the rocket may be sidestepped.

$$\begin{bmatrix} \overrightarrow{F_{ext}} & , & \overrightarrow{M_{ext}} \end{bmatrix} = \begin{bmatrix} \frac{dm\overrightarrow{v_b}}{dt} + \overrightarrow{\omega_b}\times m\overrightarrow{v_b} & , & \frac{d\overrightarrow{L_b}}{dt} + \overrightarrow{\omega_b}\times\overrightarrow{L_b} \end{bmatrix} \tag{5}$$

2.3 Sensors

An IMU sensor is introduced to track the navigation of the rocket. The motivation for introducing this system is to avoid jamming from external sources, while allowing a good performance.

The sensor is modeled by means of a bias and a random noise, which are added to the calculated position and attitude. Note that when these kind of systems are employed for short trajectories, accuracy must be on the order of magnitude of 0.1 mili-g (where g is the modulus of gravity acceleration) for accelerometers and 0.01 degrees per second for angular speeds.

3 GUIDANCE, NAVIGATION AND CONTROL

This section describes the proposed guidance, navigation and control (GNC) algorithms.

3.1 Navigation

Navigation process refers to the determination of the rocket position and attitude as well as the target position and velocity during the whole trajectory. The aim is to obtain rocket angular parameters and the line of sight between rocket and target.

Using mechanization equations, the IMU calculates position, velocity, and attitude vectors by integrating accelerations and angular velocities in body axes. (Britting 1971). Consequently, wind angles, namely bank (μ), flight path (γ) and heading (χ), can be obtained from velocity vector and Euler angles (ϕ, ψ, θ) (Hull et al. 2007). The Mach number (M) can also be estimated using the ISA model (International Organization for Standardization 1975), together with position, and velocity vector.

Line of sight $(\overrightarrow{LOS_e})$ may be calculated in earth axes by subtracting rocket position $(\overrightarrow{r_e})$, determined by IMU sensors, from target position $\overrightarrow{tp_e}$, which may be communicated to the GNC system, e.g., by a external data link in the launcher.

3.2 Guidance Law

A modified proportional law is proposed for the guidance of the rocket. Guidance is only activated when the rocket has burnt the fuel on board (de Celis et al. 2017). The mathematical expression for the proposed guidance is described by equation 6:

$$\begin{bmatrix} n_{dem_h} \\ n_{dem_v} \end{bmatrix} = N \begin{bmatrix} \frac{d}{dt}\left[atan\left(\frac{\overrightarrow{LOS_e}\cdot\overrightarrow{j_e}}{\overrightarrow{LOS_e}\cdot\overrightarrow{i_e}}\right)\right] - \dot{\chi} \\ \frac{d}{dt}\left[atan\left(\frac{\overrightarrow{LOS_e}\cdot\overrightarrow{k_e}}{\overrightarrow{LOS_e}\cdot\overrightarrow{i_e}}\right)\right] - \dot{\gamma} \end{bmatrix} ||\dot{\overrightarrow{LOS_e}}||, \tag{6}$$

where n_{dem_h} and n_{dem_v} are horizontal and vertical demanded load factors, respectively, expressed in body axes and, N is the proportional navigation constant, which has been set to three (note that this value has been obtained from experimental results).

3.3 Control System

The proposed control system is based on modern control theory. Its bases are as follows. Firstly, the system is linearized on the working point. Secondly, a closed loop feedback, which features tuneable gains, is implemented. Thirdly, a neural network is implemented to aid the system finding the most suitable gains to keep high levels of stability and performance. Finally, the actuator strategy is presented.

3.3.1 Linearization

The system is linearized at each of the Mach numbers in Table 2. It is also linearized at five different points during rocket fuel burn, i.e., for different rocket masses. When linearizing equations 1, 2, 3, 4, and 5, the following assumptions hold:

- Rocket movement is restricted to the horizontal $(X_e - Y_e)$ plane.
- The body of the rocket is axis-symmetrically perfect.
- Flight angles are small enough such that trigonometric functions may be linearized.

Note that due to the geometry of the rocket, which is axis-symmetric, the linearization of the equations of motion is only presented for one of the planes of motion, i.e, the horizontal plane. Consequently, equations 7 approximate rocket motion in the horizontal plane:

$$\begin{gathered} \rho V^2 S\left(C_{L_\alpha}(M)\alpha + \tfrac{d}{2V}C_{Nq}(M)\dot{\psi} + \tfrac{d}{2V}C_{Nq}(M)\dot{\alpha} + C_{N\delta}\delta\right) = 2m(t)\cdot V\cdot\dot{\chi} \\ \rho V^2 Sd\left(C_{M_\alpha}(M)\alpha + \tfrac{d}{2V}C_{M_q}(M)\dot{\psi} + \tfrac{d}{2V}C_{M_q}(M)\dot{\alpha} + C_{N\delta}(M)\tfrac{C_{M_\alpha}(M)}{C_{L_\alpha}(M)}\delta\right) = 2I_y(t)\ddot{\psi} \\ \psi - \chi = \alpha \\ \dot{\psi} - \dot{\chi} = \dot{\alpha}, \end{gathered} \tag{7}$$

where V is rocket speed (note that $V = aM$, where a is the speed of sound), and α is the angle of attack (the rest of variables have been previously defined).

The equations in 7 can be rewritten as a matrix equation, as it is shown in 8:

$$\begin{bmatrix} \dot{\chi} \\ \dot{\psi} \\ \ddot{\psi} \end{bmatrix} = \begin{bmatrix} A_1(M,t) & A_2(M,t) & A_3(M,t) \\ 0 & 0 & 1 \\ A_4(M,t) & A_5(M,t) & A_6(M,t) \end{bmatrix} \begin{bmatrix} \chi \\ \psi \\ \dot{\psi} \end{bmatrix} + \begin{bmatrix} B_1(M,t) \\ 0 \\ B_2(M,t) \end{bmatrix} [\delta] - \rightarrow \dot{X_p} = A_p(M,t)\overrightarrow{X_p} + B_p(M,t)\overrightarrow{U_p} \quad (8)$$

where A_i and B_j are functions aerodynamic coefficients and mass for $i = 1,...,6$ and $j = 1,2$, which basically means they are functions of Mach number and time.

In rocket guidance, command input to the control system is usually a load factor, n_{dem}, which may be expressed as a function of $\dot{\chi}$: $n_{dem} = \dot{\chi}V/g$. Note that load factors may be measured by the accelerometers in the IMU. Similarly, ψ and its derivative can be measured by the IMU. From n, ψ and $\dot{\psi}$, $\dot{\chi}$ can be easily determined (Hull et al. 2007). The equation of measurements in 9 allows its calculation.

$$\begin{bmatrix} n \\ \psi \\ \dot{\psi} \end{bmatrix} = \begin{bmatrix} \frac{V}{g}A_1(M,t) & \frac{V}{g}A_2(M,t) & \frac{V}{g}A_3(M,t) \\ 0 & 1 & 0 \\ 0 & 0 & 1 \end{bmatrix} \begin{bmatrix} \chi \\ \psi \\ \dot{\psi} \end{bmatrix} + \begin{bmatrix} \frac{V}{g}B_1(M,t) \\ 0 \\ 0 \end{bmatrix} [\delta] - \rightarrow \overrightarrow{Y_p} = C_p\overrightarrow{X_p} + D_p\overrightarrow{U_p} \quad (9)$$

3.3.2 Closed-loop Feedback System

Analyzing the system in 8, three poles may be identified. Consequently, a modern theory based closed-loop controller is proposed. Its scheme is shown in Figure 3.

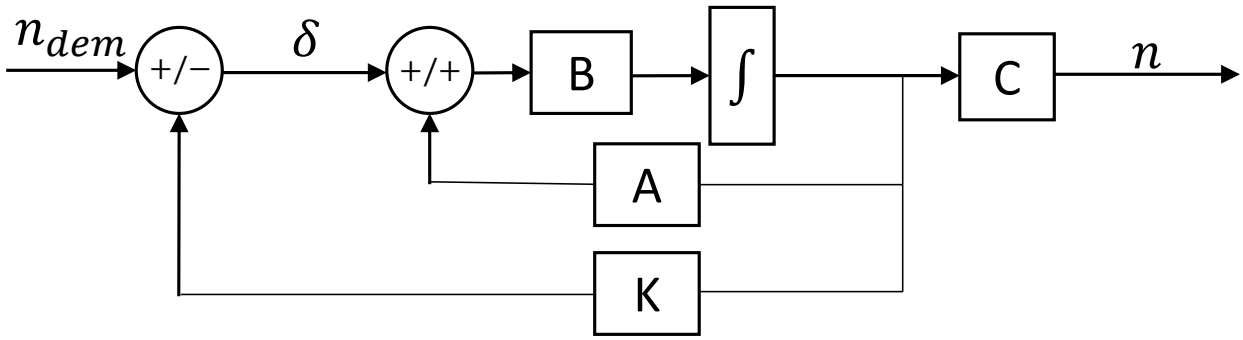

Figure 3: Closed-loop feedback scheme.

Robust pole placement techniques are used to determine the values of K in the linearization points (see Chilali et al. (1999) for more details on this). After that, to determine the values of the controller constant matrix K outside the linearization points, and to provide a self-programming method, the following machine learning techniques, which are based on neural networks, are implemented.

3.3.3 Neural Network

The calculation of K outside the linearization points is based on neural networks. The aim is to get a high accuracy on its determination process by combining the calculated values at the linearization points with a self-learning process.

Machine Learning techniques have already been used in both traditional and modern GNC applications (see Yu et al. (2004), Jankovic et al. (2016), Mohamed and Dongare (2018), Villa et al. (2020)). Regarding neural networks, its main advantage against other approximations consists of their ability to learn flight dynamics equations. This capability enables flight prediction without knowledge of the application's

physics (Yadav et al. 2015). Therefore, it is possible to replicate the determination process of K outside the predefined operating points. It should be noted that the use of neural networks to solve nonlinear equations, even when there is uncertainty, has been demonstrated to be successful (Yadav et al. 2015).

A neural network is employed to estimate the values in the K matrix to be used in the controller closed-loop. The network features two-layers with one hundred standard sigmoid hidden neurons and a linear output neuron. The number and shape of neurons, as well as the amount of training and validation data chosen, are based on a review of the literature (specifically Yadav et al. (2015)) and a hyperparametric study. As a result, the number of 100 was obtained to be significant as the number of neurons, while sigmoid activation functions were employed. Other settings were tested. However, the obtained results were significantly worse (by more than a 10%) as compared to the results provided by the proposed settings.

The input vector of the neural network is composed of two components, time and Mach number. The target is composed of all the components of the K matrix, i.e., $K_{1,1}$, $K_{1,2}$, and $K_{1,3}$. Consequently, the training aims at replicating flight dynamics: for each time instant and Mach number of flight, the optimal values for $K_{1,1}$, $K_{1,2}$, and $K_{1,3}$ are to be calculated. Table 3 shows an example of the available 10^8 rows of data, which are obtained from ten thousand shot simulations, where initial and contour conditions are varied to minimize bias and avoid overfitting. The architecture of proposed neural network is showed in Figure 4.

Levenberg-Marquardt backpropagation algorithm is used to train the network with 70% of the available data, which is presented to the network during training, and the network is adjusted according to its error (Kanzow et al. 2005). Note that a representative amount of input and target data are left aside for validation purposes. In this case, as current practice, 15% of the available data is used to measure network generalization, and to halt training when generalization stops improving. Finally, the remaining 15% is left for testing, which has no effect on training and so provides an independent measure of network performance during and after training.

The performance of the training algorithm can be quantified by means of the Mean Squared Error (MSE) and the Regression (R^2) parameter values. The MSE is defined as the average squared difference between the outputs and the targets. Lower values are preferable. There is no error if the value is zero. R^2 values quantify the relationship between outputs and goals. An R^2 value of one indicates a close relationship, while a value of 0 indicates a random relationship. Other indicators (such as Mean Average Error, MAE) can also be used to monitor and validate the training while over-fitting is avoided. The training process is considered complete when the MSE stops improving.

After 1000 iterations and a validation process, a MSE value of $2.1 \cdot 10^{-4}$ and a R^2 value of 0.997 are obtained. As shown in the numerical simulations in the next section, these results are sufficient for the studied application, as circle error probable is reduced. In addition, the trained neural network is tested with the independent data (15% of the collected data), producing similar MSE and R^2 values.

Table 3: Neural network input and target values.

Inputs		Target		
$t(s)$	$Mach$	$K_{1,1}$	$K_{1,2}$	$K_{1,3}$
0.700	0.7668	0.0291	-0.5542	0.856
1.011	0.006	-0.711	0.006	0.824
...	...	...	...	...

3.3.4 Actuator Strategy

Previous two dimensional controller is implemented twice, i.e., for vertical and horizontal control. Controller outputs, which are canard deflections, are set to be a specific value before fuel burnt is ended. During fuel burn horizontal canard deflection is set to 0 and vertical is set to a fixed value, which varies depending on

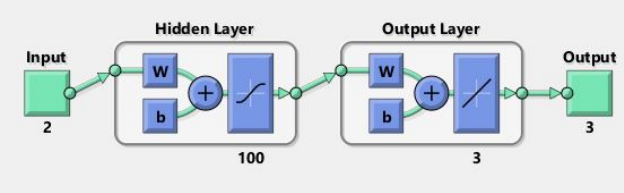

Figure 4: Neural network scheme.

target location according to a linear law. The further the target is, the higher the initial canard deflection. This approximation has been done to set the rocket initial launch angle as a constant.

4 NUMERICAL SIMULATIONS

The proposed nonlinear equations of motion are integrated forward in time. A fixed time step Runge-Kutta scheme of fourth order is used to obtain a single flight trajectory. The validation of this approach for ballistic flights is shown in de Celis et al. (2017). To demonstrate the accuracy of the results provided by the proposed novel approach, which is based on neural networks, they are compared to the results obtained from a conventional controller method, e.g., the one in de Celis et al. (2017). MATLAB/Simulink R2020a on a desktop computer with a Intel i9 processor and 32 GB RAM is employed in the simulations.

The rest of this section is divided in three subsections. Firstly, non controlled ballistic trajectories are presented. Secondly, controlled Monte Carlo simulations are showed. Finally, comparison of conventional controller against the proposed solution here is conducted.

4.1 Ballistic Trajectories

To test the developed algorithms, three nominal trajectories will be employed. A total of 10,000 simulations are conducted. Nominal impact points are set to 750 m, 850 m, and 950 m. In order to reach these ranges, initial shot angles have been set using artillery shot tables for projectile. Initial lateral correction is set to compensate Coriolis and gyroscopic forces. Results of the simulations are shown in Figure 5. Each of the three subplots represents, from left to right, the ballistic shots trajectories for impact points at 750 m, 850 m, and 950 m, respectively. As it can be observed, dispersion at impact point is significant. Numeric results are shown in Table 5.

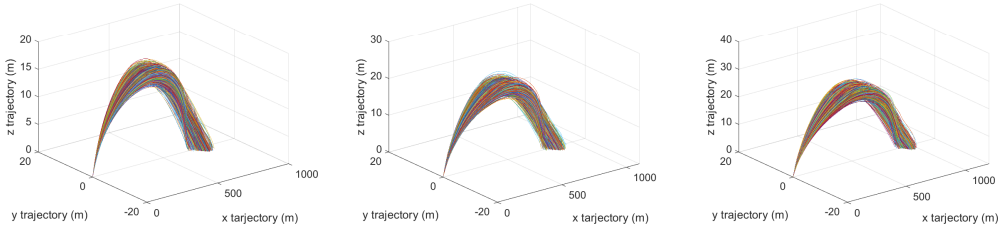

Figure 5: Ballistic flights for different impact points.

4.2 Monte Carlo Simulations

Monte Carlo analysis is conducted to determine closed-loop performance across a full spectrum of uncertainty at initial conditions, sensor data acquisition, atmospheric conditions, thrust properties and aerodynamic coefficients. Uncertainty in aerodynamic coefficients should always be carefully addressed. Aerodynamics are usually modelled by means of analytical and simulation methods, with limited experimentation, and accuracy of estimated values could slightly differ from reality, but in any case controller is designed to avoid this problem. Uncertainty model details are provided in Table 4, where Nom. stands for nominal

value. Note that uncertainty model for sensors is defined in Section 2.3. A set of 10,000 shots is performed for each of the following: ballistic shots, conventional controller shots and neural network based controller shots. Then, a total of 30,000 simulations are performed. Note that this simulation campaign is different from one employed for neural network training.

Table 4: Monte Carlo simulation parameters.

Parameter (deg)	Initial ϕ	Initial Pitch	Wind Speed	Wind Direction	Thrust	Initial azimuth
Mean	0°	Nom.	10 m/s	0°	T(t)	Nom.
Standard Deviation	20°	0.01°	5 m/s	20°	10 N	0.01°
Parameter (deg)	$C_{D_0}(M)$	$C_{D_{\alpha^2}}(M)$	$C_{L_\alpha}(M)$	$C_{L_{\alpha^3}}(M)$	$C_{mf}(M)$	$C_{Nq}(M)$
Mean	Nom.	Nom.	Nom.	Nom.	Nom.	Nom.
Standard Deviation	10% of Nom.	5% Nom.	10% of Nom.	5% of Nom.	10% of Nom.	10% of Nom.
Parameter (deg)	$C_{M_\alpha}(M)$	$C_{M_{\alpha^3}}(M)$	$C_{M_q}(M)$	$C_{mm}(M)$	$C_{spin}(M)$	$C_{N\delta}(M)$
Mean	Nom	Nom.	Nom.	Nom.	Nom.	Nom.
Standard Deviation	10% of Nom.	5% of Nom.	10% of Nom.	10% of Nom.	10% of Nom.	10% of Nom.

4.3 Discussion

Results for ballistic trajectories, neural network based controller and conventional controller approaches are shown in Figure 5, Figure 6 and Figure 7, respectively. Each of them are composed of three sub-figures, representing trajectories, from left to right, for impact points set to 750 m, 850 m, and 950 m. Note that controlled flights are only IMU assisted. The circular error probable (CEP) for each of the impact points and for each of the trajectories, namely ballistic, conventional controller and neural network based controller, are shown in Table 5. Note that even with an conventional or neural network based controllers, there are still errors associated to the aerodynamic response of the rocket. As a general remark, controlled flights exhibit tighter impact groupings, getting similar results for both controllers. Note that improvements or reductions on the CEP of 99% are obtained. The main advantage of the proposed approach is that it can achieve high levels of precision in the presence of uncertainty and disturbances without the use of expensive components.

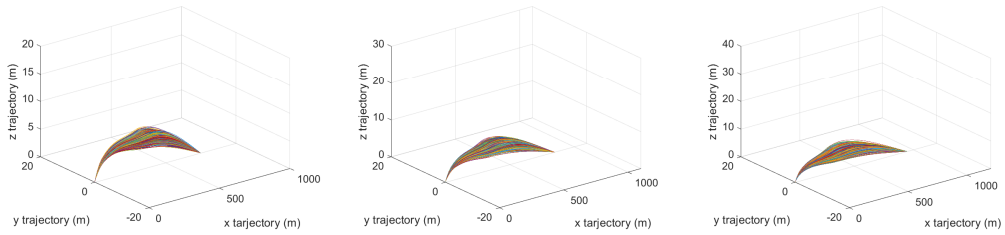

Figure 6: Detailed shots for neural network controlled trajectories.

Table 5: Circular Error Probable for different algorithms.

Nom. Impact Point (m)	Ballistic (m)	Conventional controller (m)	Neural network Controller (m)
750	124.27	0.54	0.55
850	127.44	0.51	0.50
950	131.18	0.58	0.52

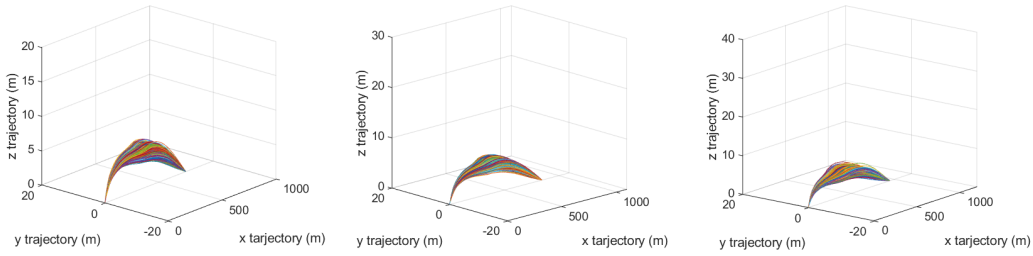

Figure 7: Detailed shots for conventional controlled trajectories.

5 CONCLUSIONS

A novel approach has been developed that is based on an innovative neural network-based controller. The proposed method aims at improving the precision of man-portable air-defense systems during guidance, thereby improving the precision at the impact point. Small errors of less than one meter have been achieved in IMU systems. It is proposed to use a modified proportional navigation law, which is integrated with the previously described novel control technique based on neural networks.

The novel proposed methodology demonstrates that accuracy levels can be improved or matched when compared to other methodologies, while exhibiting higher levels of precision in the presence of uncertainty and disturbances without the use of expensive components.

Future research will focus on hardware in the loop testing. This additional testing will demonstrate in real settings the effectiveness of the presented approach. In addition, the methodology could be used in other aerial platforms. In this case, it would be necessary to reformulate the dynamics model and to recalculate all the masic and aerodynamics parameters.

ACKNOWLEDGMENT

This research was supported by Project Grants F663 - AAGNCS by the "Consejería de Ciencia, Universidades e Innovación, Comunidad de Madrid" and "Universidad Rey Juan Carlos" and PID2020-112967GB-C33 by "Ministerio de Ciencia e Innovación".

REFERENCES

Alameri, S. 2019. "Missile guidance navigation and control algorithms design using machine learning". *University of Belgrade*.

Britting, K. R. 1971. "Inertial navigation systems analysis.".

Bryne, T. H., J. M. Hansen, R. H. Rogne, N. Sokolova, T. I. Fossen, and T. A. Johansen. 2017. "Nonlinear observers for integrated INS\/GNSS navigation: implementation aspects". *IEEE Control Systems Magazine* 37(3):59–86.

Chilali, M., P. Gahinet, and P. Apkarian. 1999. "Robust pole placement in LMI regions". *IEEE transactions on Automatic Control* 44(12):2257–2270.

Creagh, M. A., and D. J. Mee. 2010. "Attitude guidance for spinning vehicles with independent pitch and yaw control". *Journal of guidance, control, and dynamics* 33(3):915–922.

de Celis, R., and L. Cadarso. 2018. "GNSS/IMU laser quadrant detector hybridization techniques for artillery rocket guidance". *Nonlinear Dynamics* 91(4):2683–2698.

de Celis, R., and L. Cadarso. 2019. "Spot-Centroid Determination Algorithms in Semiactive Laser Photodiodes for Artillery Applications". *Journal of Sensors* 2019.

de Celis, R., L. Cadarso, and J. Sánchez. 2017. "Guidance and control for high dynamic rotating artillery rockets". *Aerospace Science and Technology* 64:204–212.

Diwani, D., A. Chougule, and D. Mukhopadhyay. 2020. "Artificial Intelligence based Missile Guidance System". In *2020 7th International Conference on Signal Processing and Integrated Networks (SPIN)*, 873–878. IEEE.

Hamilton, R. 1995. "Precision guided munitions and the new era of warfare". *Air Power Studies Centre, Royal Australian Air. DOI: http://fas. org/man/dod-101/sys/smart/docs/paper53. htm*.

Hull, D. G. et al. 2007. *Fundamentals of airplane flight mechanics*, Volume 19. Springer.

International Organization for Standardization 1975. "ISO 2533: 1975 standard atmosphere".

Jankovic, M., J. Paul, and F. Kirchner. 2016. "GNC architecture for autonomous robotic capture of a non-cooperative target: preliminary concept design". *Advances in Space Research* 57(8):1715–1736.

Kanzow, C., N. Yamashita, and M. Fukushima. 2005. "Withdrawn: Levenberg–marquardt methods with strong local convergence properties for solving nonlinear equations with convex constraints". *Journal of Computational and Applied Mathematics* 173(2):321–343.

Lechevin, N., and C. A. Rabbath. 2012. "Robust discrete-time proportional-derivative navigation guidance". *Journal of guidance, control, and dynamics* 35(3):1007–1013.

Lee, H.-I., B.-C. Sun, M.-J. Tahk, and H. Lee. 2001. "Control design of spinning rockets based on co-evolutionary optimization". *Control Engineering Practice* 9(2):149–157.

Mohamed, M., and V. Dongare. 2018. "Aircraft neural modeling and parameter estimation using neural partial differentiation". *Aircraft Engineering and Aerospace Technology* 90(5):764–778.

Nesline, F. W., and P. Zarchan. 1985. "Line-of-sight reconstruction for faster homing guidance". *Journal of Guidance, Control, and Dynamics* 8(1):3–8.

Nguyen, N. V., M. Tyan, and J.-W. Lee. 2016. "Efficient Framework for Missile Design and 6DoF Simulation using Multi-fidelity Analysis and Data Fusion". In *17th AIAA/ISSMO Multidisciplinary Analysis and Optimization Conference*. June 13th-17th, Washington, D.C., U.S.A., 3365.

Satir, A. S., U. Demir, G. G. Sever, and N. K. Ure. 2021. "Nonlinear Model Based Guidance with Deep Learning Based Target Trajectory Prediction Against Aerial Agile Attack Patterns". *arXiv preprint arXiv:2104.02491*.

Schmidt, G. T., and R. E. Phillips. 2011. "INS/GPS integration architecture performance comparisons". *NATO RTO lecture series, low-cost navigation sensors and integration technology RTO-EN-SET-116*.

Solano-López, P., R. de Celis, M. Fuentes, L. Cadarso, and A. Barea. 2019. "Strategies for high performance GNSS/IMU Guidance, Navigation and Control of Rocketry". In *8th European Conference for Aeronautics and Space Sciences*. July 1st-3rd, Madrid, Spain.

Theodoulis, S., V. Gassmann, P. Wernert, L. Dritsas, I. Kitsios, and A. Tzes. 2013. "Guidance and control design for a class of spin-stabilized fin-controlled projectiles". *Journal of Guidance, Control, and Dynamics* 36(2):517–531.

Villa, J., J. Taipalmaa, M. Gerasimenko, A. Pyattaev, M. Ukonaho, H. Zhang, J. Raitoharju, N. Passalis, A. Perttula, J. Aaltonen et al. 2020. "aColor: Mechatronics, Machine Learning, and Communications in an Unmanned Surface Vehicle". In *Proceedings of 8th Transport Research Arena TRA 2020*. April 27th-30th, Helsinki, Finland.

Waltz, E. L., and D. M. Buede. 1986. "Data fusion and decision support for command and control". *IEEE Transactions on Systems, Man, and Cybernetics* 16(6):865–879.

Wang, X., J. Wang, and G. Gao. 2015. "Partial integrated missile guidance and control with state observer". *Nonlinear Dynamics* 79(4):2497–2514.

Yadav, N., A. Yadav, and M. Kumar. 2015. *An introduction to neural network methods for differential equations*. 1st ed. Dordrecht, Netherlands: Springer.

Yu, J.-Y., Y.-A. Zhang, and W.-J. Gu. 2004. "An approach to integrated guidance/autopilot design for missiles based on terminal sliding mode control". In *Proceedings of 2004 International Conference on Machine Learning and Cybernetics (IEEE Cat. No. 04EX826)*, edited by IEEE, Volume 1. New York, U.S.A: IEEE.

Zhang, X., Z. Yang, T. Sun, H. Yang, K. Han, and B. Hu. 2017. "Optical system design with common aperture for mid-infrared and laser composite guidance". In *Second International Conference on Photonics and Optical Engineering*, Volume 10256, 102560S. International Society for Optics and Photonics.

Zhang, Y., M. Sun, and Z. Chen. 2012. "Finite-time convergent guidance law with impact angle constraint based on sliding-mode control". *Nonlinear Dynamics* 70(1):619–625.

Zhao, J., and R. Zhou. 2015. "Unified approach to cooperative guidance laws against stationary and maneuvering targets". *Nonlinear Dynamics* 81(4):1635–1647.

AUTHOR BIOGRAPHIES

RAUL DE CELIS is an associate professor in aerospace area at Rey Juan Carlos University. He received his Ph.D. degree from Universidad Rey Juan Carlos in December 2017. His research interests are model development of aeronautic systems and navigation and control for aerial platforms. His email address is raul.decelis@urjc.es.

LUIS CADARSO is an associate professor in aerospace area at Rey Juan Carlos University. He received the Ph.D. degree in Aerospace Engineering from the Technical University of Madrid, Spain. His research interests include operations research , navigation, and control for aerial platforms. His email address is luis.cadarso@urjc.es.